First-Principles Study of CO Adsorption and Oxidation on Ru-Doped CeO2(111) Surface

ARTICLE *in* THE JOURNAL OF PHYSICAL CHEMISTRY C · MARCH 2012

Impact Factor: 4.77 · DOI: 10.1021/jp210864m

1 AUTHOR:

Hsin-Tsung Chen
Chung Yuan Christian University
78 PUBLICATIONS **698** CITATIONS

THE JOURNAL OF PHYSICAL CHEMISTRY C

Article

pubs.acs.org/JPCC

First-Principles Study of CO Adsorption and Oxidation on Ru-Doped CeO_2(111) Surface

Hsin-Tsung Chen*

Department of Chemistry, Chung Yuan Christian University, Chungli 32023, Taiwan

ABSTRACT: The interaction and mechanism for CO oxidation on a Ru-modified CeO_2 surface have been investigated by using periodic density functional theory calculations corrected with the on-site Coulomb interaction via a Hubbard term (DFT + U). Our calculations showed that (i) the Ru dopant facilitates oxygen vacancy formation, while the Ru adatoms may suppress oxygen vacancy formation. (ii) Physisorbed CO, physisorbed CO_2, and chemisorbed CO (carbonite, CO_2^-) species are observed on the Ru-doped CeO_2(111) surface; in contrast, only physisorbed CO is found on the clean CeO_2(111) surface. The vibrational frequency calculations are carried to characterize these species. (iii) Incorporating Ru ions into the ceria lattice as substitutional point defects can instead sustain a full catalytic cycle for CO oxidation and catalyst regeneration. The Ru dopant promotes CO oxidation without any activation energy leading to O vacancy formation and CO_2 desorption. Molecular O_2 adsorbs at the O vacancy forming O adspecies that then drive CO oxidation and recover the stoichiometric Ru-doped CeO_2 surface. The Bader charge analysis is carried to characterize the oxidation state of Ru ions along the catalytic cycle.

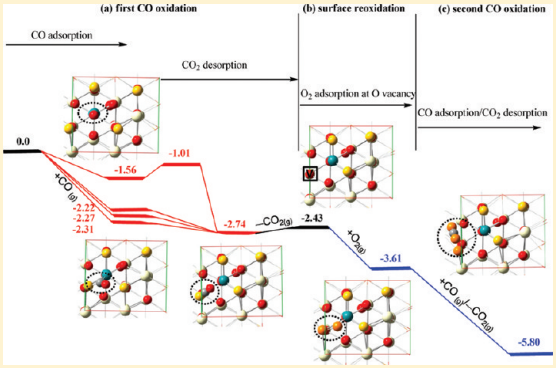

1. INTRODUCTION

Low-temperature CO oxidation is needed and important in many processes, such as automotive exhaust purification and preferential CO oxidation.[1−4] Ceria (CeO_2) is one of the most efficient catalysts due to its unique oxygen storage properties.[5] However, pure ceria cannot satisfactorily fulfill the elevated activity demands for the CO oxidation catalyst owing to its limited oxygen storage capacity (OSC) and its insufficient thermal stability. Several experimental[6] and theoretical[7−9] studies have demonstrated the surface selectivity for the CO oxidation and showed that CO does not adsorb on the stoichiometric CeO_2(111) surface. One of the effective strategies to tackle these problems is to modify ceria with other metal elements. Shapovalov and Metiu[10] and Camellone and Fabris[11] showed that the (111) surface of ceria can be made reactive to CO oxidation by doping of the surface with Au theoretically. Yang et al.[12] also showed the same behavior on the Cu-doped CeO_2(111) surface using the DFT + U methods. Recently, studies of Ti-, Zr-, and Hf-doped CeO_2(110) surfaces reported by Nolan[13] and La-doped (111) and (110) surfaces reported by Yeriskin and Nolan[14] have shown that these are more reactive to CO adsorption than the undoped surfaces. The enhancement for CO oxidation by the doping of CeO_2 with other metals have also been evidenced by the experimental investigations.[15−19]

The reactivity of the modified ceria catalysts is controlled by several factors, such as the size of the metal particle, the pretreatment conditions resulting in different morphology of the catalysts, and the interaction between adding metal and the oxide. As a result, the nature of the active sites on the doping of ceria with other metals and the reaction mechanisms for CO oxidation are still subjects of debate. Higher OSC of $Ce_{1-x}Ru_xO_2$ (x = 0.05, 0.10) catalysts have been synthesized and characterized in the literature by Singh and Hegde[20] who showed that $Ce_{1-x}Ru_xO_2$ materials have high CO oxidation activity at low temperature. The oxidation state of Ru in the $Ce_{1-x}Ru_xO_2$ may play a curial role during the CO oxidation reaction. From X-ray photoelectron spectra (XPS) study, the presence of Ru^{4+} ions of the $Ce_{1-x}Ru_xO_{2-\delta}$ catalysts has been identified.[20] A higher percentage of CO to CO_2 conversion in the absence of feed oxygen gas suggests lattice oxygen is activated by Ru ion substitution in CeO_2 and that feed oxygen can be reversibly exchanged with lattice oxygen, resulting in lower-temperature CO oxidation. Thus synergistic electronic interaction between the redox couples (Ru^{4+}/ Ru^{3+} and Ce^{4+}/ Ce^{3+}) plays an important role in enhancing the activity of CO oxidation. To the best of our knowledge, no molecular level study on CO oxidation on Ru-doped CeO_2 catalysts is available, although understanding of the detailed reaction mechanism at the molecular level is very vital for the rational design of novel catalysts for the low-temperature CO oxidation.

In the present work, we attempt to address the CO adsorption and the detailed reaction mechanisms of CO oxidation catalyzed by Ru-doped CeO_2(111). The oxidation states of Ru ions of these catalysts are also characterized. In addition, the step of healing the oxygen vacancies by molecular

Received: November 11, 2011
Revised: January 29, 2012
Published: February 15, 2012

dx.doi.org/10.1021/jp210864m | J. Phys. Chem. C 2012, 116, 6239−6246

oxygen is studied to complete a full catalytic cycle for CO oxidation.

The article is organized as follows. The computational details are presented in section 2. The calculated results including the oxygen formation energy of Ru-doped CeO_2 system, the interaction of Ru adatoms with the stoichometric $CeO_2(111)$ surface, the adsorption of CO on these surfaces, and the relevant mechanisms for CO oxidation are presented in section 3. A brief summary is given in section 4.

2. COMPUTATIONAL METHODS

We applied spin-polarized density functional theory (DFT) plane wave calculations as implemented in the Vienna ab initio simulation package (VASP)[21,22] with the projector augmented wave method (PAW).[23] The generalized gradient approximation (GGA) with the Perdew–Wang 91 (PW91) exchange-correlation functional[24–26] was used. The calculations were carried out using the Brillouim zone sampled with $(3 \times 3 \times 3)$ and $(3 \times 3 \times 1)$ Monkhorst-Pack[27] mesh *k*-points grid for bulk and surface calculations, respectively, and with a cutoff energy of 400 eV, which allows to be converged to 0.01 eV in the total energy. Since regular DFT methods are unable to describe the localization of the Ce_{4f} states in the reduced ceria,[28–31] the DFT with the Hubbard *U* term (DFT + *U*) method[32] was applied in order to accurately correct the strong on-site Coulomb interactions of Ce_{4f} states.[28–31,33] The issues with regard to DFT + *U* and the selected value of *U* parameters have been discussed extensively. However, there is no general rule on a correct *U* value to describe the localized 4*f* orbitals of Ce. The proposed *U* values seem to depend on the oxidation states of Ce and the functional used. For example, Loschen et al.[34] proposed a well-balanced *U* value of 5–6 eV for LDA + *U* calculations and 2–3 eV for GGA + *U* calculations. Andersson et al.[35] clarified that the *U* value must satisfy the criteria of $U > 6$ eV for LDA calculations and $U > 5$ eV for GGA calculations to exactly predict the ground state of Ce_2O_x. As such, we chose $U = 6.3$ eV in the present study.[36–39] In test calculations on the oxygen vacancy formation energy (E_f) for CeO_2 bulk, the calculated E_f is 3.20 eV with $U = 6.3$ eV, which is very close to the values of 3.15 and 3.19 eV with $U = 5$ and 6.1 eV. In addition, the predicted energy gaps of $O_{2p} \rightarrow Ce_{4f}$ and $O_{2p} \rightarrow Ce_{5d}$ for the CeO_2 are 2.4 and 5.5 eV, respectively, which are better in agreement with the experimental values[40–42] of 2.54–3.0 and 6.0 eV compared with the DFT results (1.8 and 5.5 eV).

The 12.5% Ru-doped ceria, $Ce_{0.875}Ru_{0.125}O_2$, which showed higher OSC,[20] was modeled by introducing Ru-doping atoms to substitute Ce atoms in the supercell. The reduced systems were created by removing one oxygen atom resulting in an oxygen vacancy concentration of 6.25%. For the surface model, we examined only the (111) surface to characterize the CO–$Ce_{0.875}Ru_{0.125}O_2$ interactions because the (111) surface is energetically the most stable[43–45] among the low-index $CeO_2(111)$, (110), and (100) surfaces. As shown in Figure 1, the CeO_2 and $Ce_{0.875}Ru_{0.125}O_2(111)$ surface models with 12 atomic layers, a $p(\sqrt{3} \times 2)$ lateral cell, was constructed. In order to examine the effect of Ru cation for CO oxidation, for the $Ce_{0.875}Ru_{0.125}O_2(111)$ surface, one Ce atom of the outermost Ce layer on each side of the $p(\sqrt{3} \times 2)$ CeO_2 (111) slab was replaced by a Ru atom. The bottom six layers of the surface model were fixed to the estimated bulk parameters, while the remaining layers were fully optimized. A vacuum space greater than 15 Å was introduced to prevent interactions between slabs. The adsorption energies were calculated by $\Delta E_{ads} = E[\text{surface–adsorbate}] - E[\text{surface}] - E[\text{adsorbate}]$, where $E[\text{surface–adsorbate}]$, $E[\text{surface}]$, and $E[\text{adsorbate}]$ are the calculated electronic energies of adsorbed species on the surface, the bare surface, and the adsorbate in the gas phase, respectively. The climbing image nudged elastic band (CI-NEB) method[46,47] was applied to map out MEPs after locating plausible local minima. All transition states were verified by the number of imaginary frequencies (NIMG) with NIMG = 1. The charge density difference was carried out using the expression $\Delta\rho_{diff} = \rho[\text{surface + adsorbate}] - \rho[\text{surface}] - \rho[\text{adsorbate}]$, where $\rho[\text{surface + adsorbate}]$, $\rho[\text{surface}]$, and $\rho[\text{adsorbate}]$ are the charge density of adsorbed species on the surface, the bare surface, and the adsorbate, respectively.

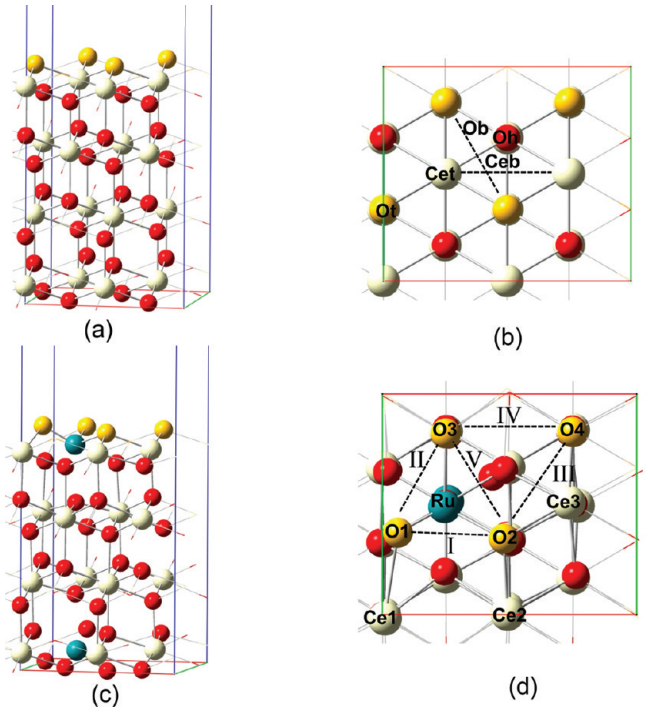

Figure 1. (a) Side and (b) top views of the $CeO_2(111)$ surface. Cet, Ceb, Ot, Ob, and Oh, corresponds to active sites for Ce top, Ce bridge, O top, O bridge, and O hollow sites, respectively. (c) Side and (d) top views of the $Ce_{0.875}Ru_{0.125}O_2(111)$ surface model. I, II, III, IV, and V corresponds to active sites for O1–O2, O1–O3, O2–O4, O3–O4, and O2–O3 sites, respectively. Yellow, red, white, and cyanine blue spheres represent the top-layer O, O, Ce, and Ru atoms, respectively. A rectangle represents the supercell used in this study.

3. RESULTS AND DISCUSSION

3.1. Ru-Doped $Ce_{0.875}Ru_{0.125}O_2$ Bulk and Surface. The geometries of stoichiometric and reduced bulk Ru-doped CeO_2 were optimized at GGA + *U* levels with and without considering spin polarization. One should note that the external (cell volume and cell shape) and internal (atomic ions and lattice parameters) degrees of freedom were allowed to relax until forces and stress vanished in the bulk calculations. The larger cutoff energy, ENCUT = 1.3 × 400 eV, and very high-accurate energy with PREC = high command were carried to avoid the Pulay stress and related problems. The predicted lattice constant of bulk 12.5% Ru-doped ceria is 5.39 Å, while that is 5.45 Å for bulk CeO_2. The theoretical values are close to the experimental values of 5.41[41] and 5.41[20] Å for bulk CeO_2 and $Ce_{0.875}Ru_{0.125}O_2$. The optimized Ce_8O_{16} unit has all Ce–O

dx.doi.org/10.1021/jp210864m | J. Phys. Chem. C 2012, 116, 6239–6246

Table 1. Lattice Constants and O Vacancy Formation Energy (E_f) of CeO_2 and $Ce_{0.875}Ru_{0.125}O_2$

	lattice constants (Å)			E_f (eV)	
species	unreduced	reduced	vacancy position	bulk	surface
CeO_2	5.45(5.41)[a]	5.50		3.20	2.08
$Ce_{0.875}Ru_{0.125}O_2$	5.39	5.46(5.41)[a]	VO1[b]	1.03, 1.58[d]	0.87
			VO2		0.33
			VO3		0.51
			VO4		1.04
			V*(O1)[c]		1.95

[a]The values in parentheses are the experimental data. [b]The labeling of the O atoms is shown in Figure 1d. VO1 means that O1 has been removed, and so on. [c]Second vacancy after VO2. [d]The different formation energies are calculated from the different coordination shell of the Ru−O bond.

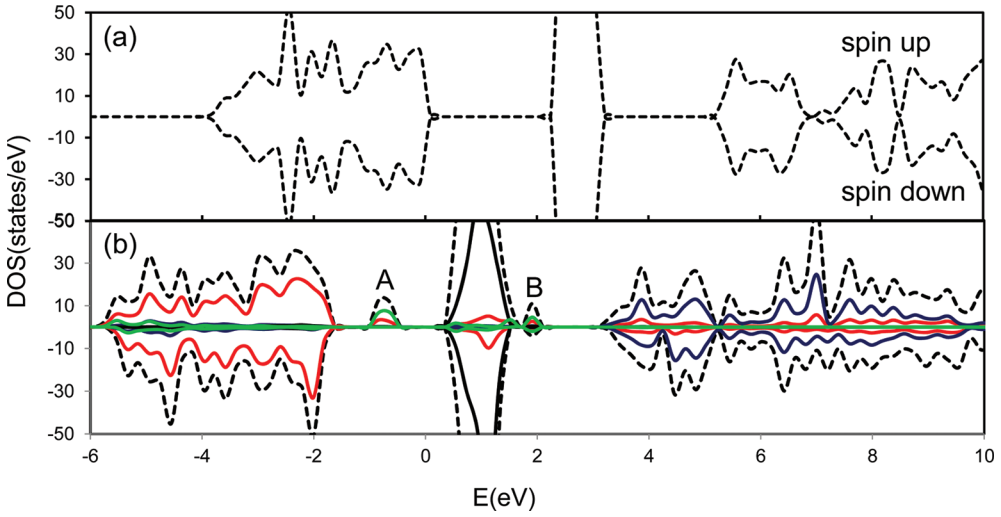

Figure 2. Density of states and local density of states for (a) $CeO_2(111)$ and (b) $Ce_{0.875}Ru_{0.125}O_2(111)$ surfaces. The black dashed, black solid, blue, red, and green lines represent total, Ce(f), Ce(d), O(p), and Ru(d), respectively. The energy at E = 0 eV represents the Fermi energy.

bond lengths equal to 2.36 Å. While optimized $Ce_{0.875}Ru_{0.125}O_2$ shows geometric distortions of the oxygen lattice with the longer Ce−O bonds average of 2.35 Å and the average of shorter Ru−O bonds 2.21 Å. Introduction of the O vacancy gives rise to significant distortions of the oxygen lattice, the Ce−O bonds get distributed over a range of 2.31 to 3.84 Å, and Ru−O bonds get distributed over a range of 2.00 to 3.30 Å.

The oxygen vacancy formation is described by the reaction of $Ce_{1-x}M_xO_2 \rightarrow Ce_{1-x}M_xO_{2-\delta} + 1/2O_2$.[48] The oxygen vacancy formation energy, E_f, was computed according to the eq 1.

$$E_f = E(Ce_{1-x}M_xO_{2-\delta}) + \frac{1}{2}E(O_2) - E(Ce_{1-x}M_xO_2) \quad (1)$$

where $E(Ce_{1-x}M_xO_2)$ indicates the energy of the bulk or surface $Ce_{1-x}M_xO_2$, $E(O_2)$ is the energy of a gas-phase O_2, and $E(Ce_{1-x}M_xO_{2-\delta})$ is the energy of the bulk in the presence of one oxygen vacancy. In the present, we only show the formation of oxygen vacancy neighboring the Ru dopant because the required energy for the vacancy further away from the Ru dopant is close to the undoped CeO_2. The calculated E_f of $Ce_{0.875}Ru_{0.125}O_2$ is 1.03 and 1.58 eV depending on the different coordination shell of the Ru−O bond.[36] Compared to CeO_2 and $Ce_{0.875}Zr_{0.125}O_2$, the smaller E_f (1.03 for $Ce_{0.875}Ru_{0.125}O_2$; 3.20 and 2.03 eV[37] for CeO_2 and $Ce_{0.875}Zr_{0.125}O_2$) indicates that $Ce_{0.875}Ru_{0.125}O_2$ shows higher OSC property than CeO_2 and $Ce_{0.875}Zr_{0.125}O_2$, which is consistent with the experimental results.[20] Thus, substitution with Ru metal ions activates lattice oxygen by the creation of longer Ce−O and Ru−O bond lengths compared to those in CeO_2 and RuO_2 metal oxides.[36]

The relaxed structure of 12.5% Ru-doped $CeO_2(111)$ surface in which two Ce atoms are replaced by two Ru atoms is shown in Figure 1c. In the structure, the Ru atom has relaxed to have six coordinations and form one short Ru−O bond length of 1.85 Å and five long Ru−O bond lengths of 2.12−2.31 Å. The lengths of short and long Ru−O bonds (1.85 and 2.12−2.31 Å) are close to that of RuO_2 (1.91 and 2.01 Å).[49] The surface O vacancy formation is calculated as shown in Table 1. The formation energies of the various nonequivalent surface oxygen of the top layer are 0.87, 0.33, 0.51, and 1.04 eV. The nearest neighbor oxygen anions (O1, O2, and O3, see Figure 1d) to Ru cations have much smaller formation energies than that for the undoped $CeO_2(111)$ surface (2.08 eV) indicating that O vacancy formation is very much facilitated by Ru doping. The formation of a second oxygen vacancy from the O1 site on the optimized surface, with an O vacancy at the O2 site already present (denoted as V*(O1)), also needs less energy with an E_f of 1.95 eV. Although it costs more to make the second vacancy than the first, the vacancy formation energy is still smaller than that of the pure surface. Thus, the Ru dopant may serve as the seed for the formation of oxygen vacancy clusters on the ceria surfaces.

The stoichometric $CeO_2(111)$ system is known to be an insulator, and the features of the electronic density of states (DOS) shown in Figure 2a are well in agreement with previous DFT + U results.[12] We find that two new features appear in the band gap, labeled A and B (Figure 2b), which are contributed

dx.doi.org/10.1021/jp210864m | J. Phys. Chem. C 2012, 116, 6239−6246

from the overlap between the Ru(d) states and the O(p) states resulting in the Ru−O binding. Interestingly, no Ce(f) state is found in the band gap indicating that no Ce^{4+} reduces to Ce^{3+}. This is corroborated by the Bader charge calculations, which are carried to characterize the oxidation states in bulk and surface $Ce_{0.875}Ru_{0.125}O_2$. In order to assign the oxidation states of Ru and Ce in the stoichiometric Ru-doped CeO_2, we did the Bader charge analyses for stoichiometric RuO_2 and CeO_2, the calculated Bader charges of Ru and Ce in the stoichiometric RuO_2 (the oxidation state of Ru is +4) and CeO_2 (the oxidation state of Ce is +4) are 5.92 and 9.60 e. The calculated Bader charges of Ru and Ce in stoichiometric bulk and surface $Ce_{0.875}Ru_{0.125}O_2$ are ∼6.14 e and ∼9.6 e, which are close to those of RuO_2 (5.92 e) and CeO_2 (9.60 e). Accordingly, in both cases, the oxidation states for Ru and Ce are characterized as +4 and +4. For reduced Ce_2O_3 (the oxidation state of reduced Ce is +3), the calculated Bader charge of reduced Ce is 9.90 e. In the reduced $Ce_{0.875}Ru_{0.125}O_{2-\delta}$, the Ru neighboring the O vacancy is still in +4 oxidation state (the Bader charge is within 6.15 and 6.17 e), while the Ce^{4+} neighboring the O vacancy is reduced to Ce^{3+} (the Bader charge is 9.90 e).

3.2. Ru/CeO_2(111) Surface. Plausible intermediates for the Ru−CeO_2 interactions were initially optimized by placing a single Ru atom at different active sites on the (111) surface, including Ce-top, O-top, Ce−Ce bridge, O−O bridge, and O-hollow, corresponding to Cet, Ot, Ceb, Ob, and Oh, respectively, as illustrated in Figure 1b. Table 2 displays the relative adsorption energies and the calculated Bader charge of Ru atom in these configurations. In all cases, the interactions between the Ru atom and the stoichiometric CeO_2(111) surface including charge transfer from the Ru atom to the surface yield the reduction of Ce ions. The most stable adsorption site for a Ru adatom was found to be the O-hollow site. The calculated adsorption energy and the Ru−O distance are −5.79 eV and 1.85 Å. The Bader charge analysis for the Ru adatom at the O-hollow site reveals that ∼1.30 e is transferred from the metal to the oxide resulting in the formation of a positively charged $Ru^{\delta+}$ with an oxidation state of +3, see Table 2. The excess charge in the oxide is mostly localized around the surface O atoms bound to Ru and on the three Ce^{4+} ions, which reduce to Ce^{3+} (the calculated Bader charge is ∼9.92 e). The vacancy formation energy of the Ru/CeO_2 system is calculated to be 3.05 eV by removing one of the three equivalent nearest neighbor surface O atoms bound to a Ru atom. This value is larger than that for pure CeO_2(111), suggesting that Ru adsorption on the CeO_2(111) surface may suppress O vacancy formation. The Ru dopant and adatom show similar behavior as Cu− and Fe−CeO_2.[12,39]

Table 2. Adsorption Energies (E_{ads}) of a Ru Adatom on the Stoichiometric CeO_2(111) Surface As Well As on an O and Ce Vacancy and the Calculated Bader Charge of a Ru Atom in These Configurations

adsorption site	E_{ads} (eV)	Ru[a]
Ce-top	−3.19	7.51($Ru^{\delta+}$)
Ce-bridge	−5.51[b]	6.71(Ru^{3+})
O-top	−3.06	7.48($Ru^{\delta+}$)
O-bridge	−4.35	7.17($Ru^{\delta+}$)
O-hollow	−5.79	6.67(Ru^{3+})
V_O	−1.46	8.19($Ru^{\delta-}$)
O-hollow (V_O)	−4.83	7.23($Ru^{\delta+}$)
V_{Ce}	−13.17	6.13(Ru^{4+})

[a]The calculated Bader charges of Ru in RuO_2 and Ru_2O_3 are 5.92 and 6.37 e, respectively. [b]The configuration of Ru at the Ce-bridge site converges to that at the O-hollow site.

In addition, the Ru adsorbed at the surface O vacancy site of the partially reduced CeO_{2-x}(111) surface is also studied. The adsorption energy is −1.46 eV, which is less stable than those for a Ru adsorbed on the stoichiometric CeO_2 (111) surface indicating that the Ru atom is not likely to occupy an O lattice site. The Bader charge analysis reveals that ∼0.2 e is transferred from the oxide to the metal resulting in the formation of a negatively charged $Ru^{\delta-}$. Accordingly, one of two Ce^{3+} is oxidized to Ce^{4+} after Ru adsorbed at the surface O vacancy. The adsorption energy of a Ru adsorbed at the O-hollow site on the partially reduced CeO_{2-x}(111) surface is calculated to be −4.83 eV. It turns out that Ru atom prefers to localize at the O-hollow site even on the partially reduced CeO_{2-x}(111) surface. According to the Bader charge analysis, the two excess electrons created by the O vacancy formation give rise to a significant charge transfer (0.55 e) from the oxide surface to Ru atom, while the remaining 1.44 e are mainly transferred to the three Ce ions in the second atomic layer of the surface. However, the adsorbed Ru atom still remains of positive charge in the Ru/CeO_{2-x} system, only except for the Ru adsorbed at the O vacancy (see Table 2).

3.2.1. CO Adsorption and Oxidation on $Ce_{0.875}Ru_{0.125}O_2$(111) Surfaces. One should note that we only discuss adsorption with the C-end toward the surface due to either not binding or binding very weakly for the adsorption O-end toward the surface. Only weak physisorption of CO on the stoichiometric CeO_2(111) is found, see Table 3. The result is consistent with the previous studies reported by Huang and Fabris,[7] Nolan and Watson,[8] and Yang et al.[9] In the present work, we explore whether the Ru-modified ceria changes this state of matters. The adsorption of a CO molecule on a Ru

Table 3. Adsorption Energies (E_{ads}) and Calculated Frequencies of a CO on the Stoichiometric CeO_2(111) and Ru-Doped CeO_2(111) Surfaces[a]

adsorption site	stoichiometric CeO_2 (eV)	frequency (cm^{-1})	Ru-doped CeO_2 (eV)	frequency (cm^{-1})
		Physisorption		
Ce1-top	−0.17	2133	−0.23	2135
Ce2-top			−0.19	2135
Ce3-top			−0.19	2157
O4-top			−0.16	2129
O2−O4	0.08	2131	−0.20	2128
O3−O4			−0.19	2112
		Chemisorption		
Ru-top			−1.56	1972
O1−O2			−2.31	1861
O1−O3			−2.22	1847
O2−O3			−2.27	1683
		CO_2 Formation		
O1-top			−2.74	2373, 1334, 633
O2-top			−2.67	2371, 1324, 618
O3-top			−2.31	2429, 1354, 607

[a]The calculated frequencies are 2136 cm^{-1} for a gas-phase CO and 2377, 1321, and 644 cm^{-1} for a gas-phase CO_2.

dx.doi.org/10.1021/jp210864m | J. Phys. Chem. C 2012, 116, 6239−6246

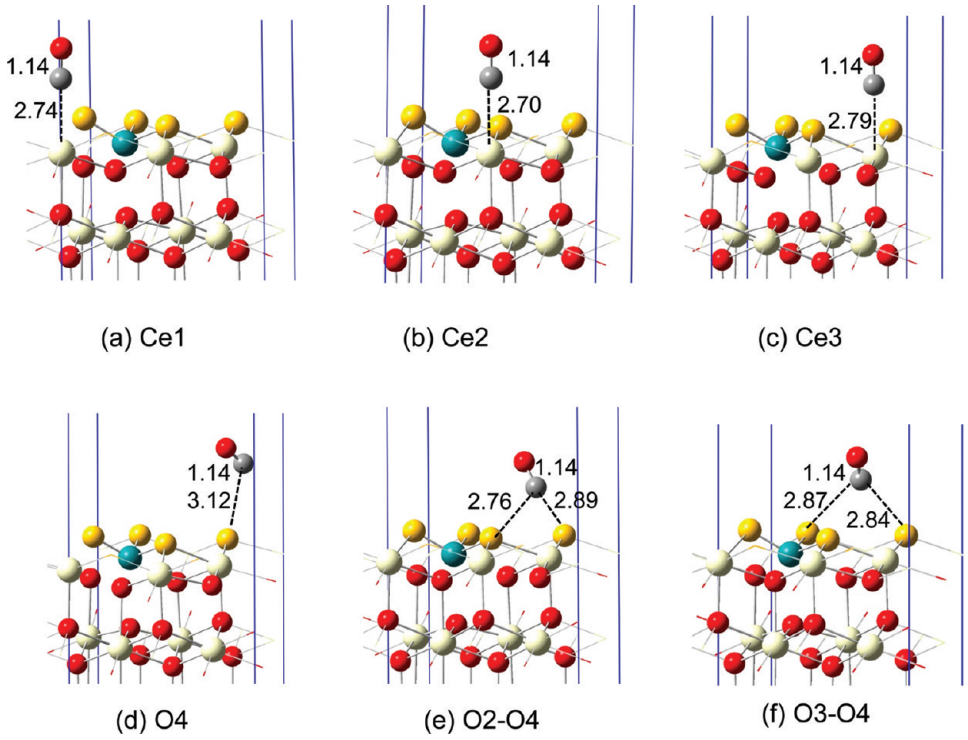

Figure 3. Side view for the optimized structures of CO physisorption on the $Ce_{0.875}Ru_{0.125}O_2(111)$ surface: (a) Ce1, (b) Ce2, (c) Ce3, (d) O4, (e) O2−O4, and (f) O3−O4.

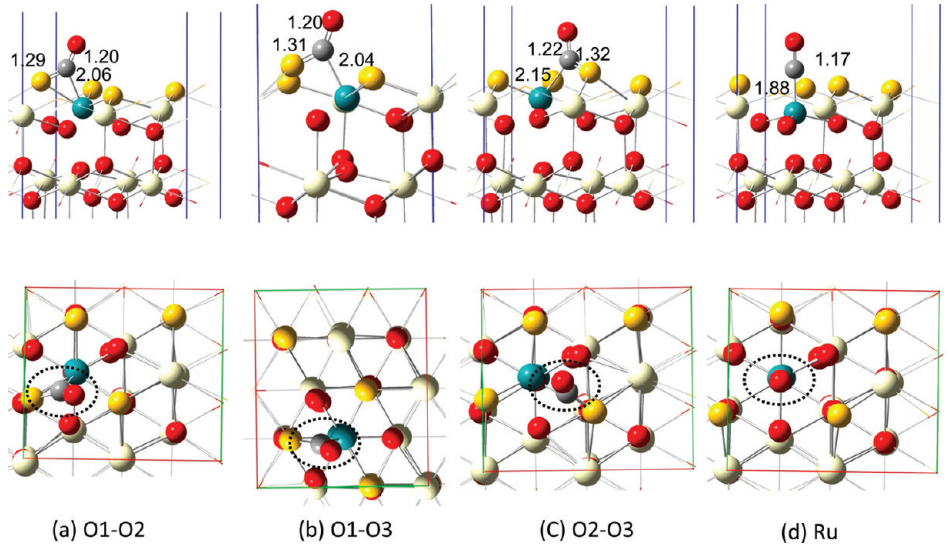

Figure 4. Side view and top view for the optimized structures of CO chemisorption on the $Ce_{0.875}Ru_{0.125}O_2(111)$ surface: (a) O1−O2, (b) O1−O3, (c) O2−O3, and (d) Ru.

adatom in the lowest-energy O-hollow site is studied. The calculated adsorption energy and frequency of the C−O are −1.97 eV and 1980 cm^{-1}. The formation of a CO_2 from the adsorption of CO at the O-hollow site of the $Ru/CeO_2(111)$ surface can be neglected due to the requirement of a high barrier of 1.04 eV. To this end, we studied the interaction of a CO molecule with the $Ce_{0.875}Ru_{0.125}O_2(111)$ surface.

To describe the interactions between a CO molecule and the $Ce_{0.875}Ru_{0.125}O_2(111)$ surface, a CO molecule is placed at the various sites on the $Ce_{0.875}Ru_{0.125}O_2(111)$ surface, including Ce-top, O-top, Ru-top, and O−O bridge sites, as seen in Figure 1d. The interactions can divide into three types of adsorption: CO physisorption, CO chemisorption, and CO_2 physisorption. The optimized configurations of CO physisorption, CO chemisorption, and CO_2 physisorption are depicted in Figures 3, 4, and 5, respectively. The adsorption energies of all optimized configurations are shown in Table 3.

CO physisorption is observed at the Ce1, Ce2, Ce3, and O4 top sites as well as at the long O-bridge sites (O2−O4 and O3−O4). As shown in Table 3, the adsorption energies are between −0.16 and −0.23 eV, which are close to those (0.08 and −0.17 eV) for the CO physisorption on the pure $CeO_2(111)$ surface. Different from the $CeO_2(111)$ surface, CO chemisorption is found to occur at the Ru top and the

dx.doi.org/10.1021/jp210864m | J. Phys. Chem. C 2012, 116, 6239−6246

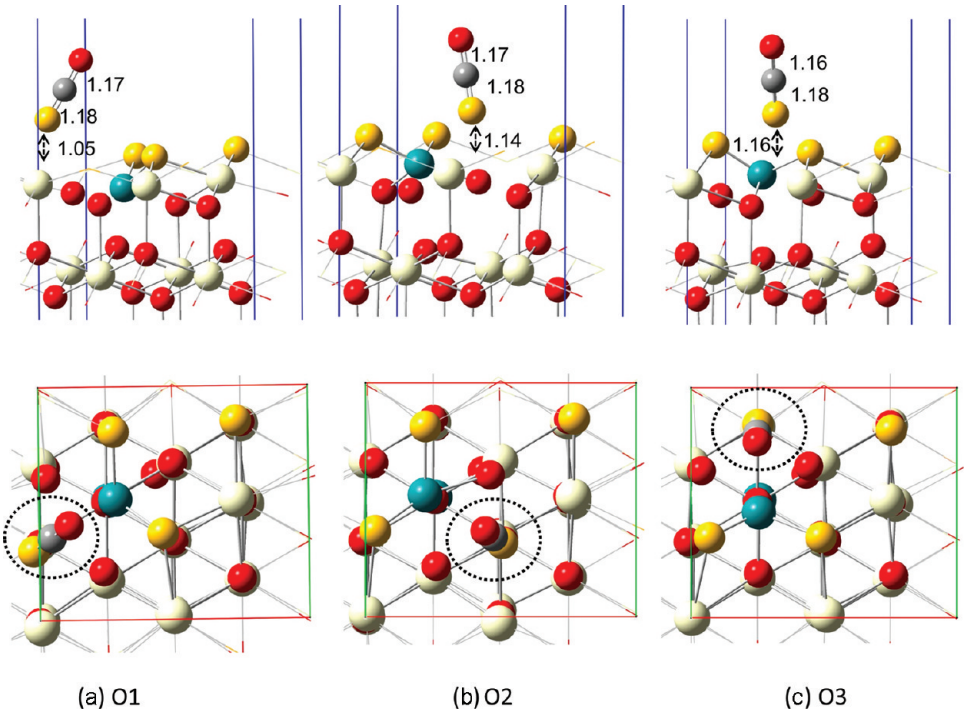

Figure 5. Side view and top view for the optimized structures of CO_2 formation on the $Ce_{0.875}Ru_{0.125}O_2(111)$ surface: (a) O1, (b) O2, and (c) O3.

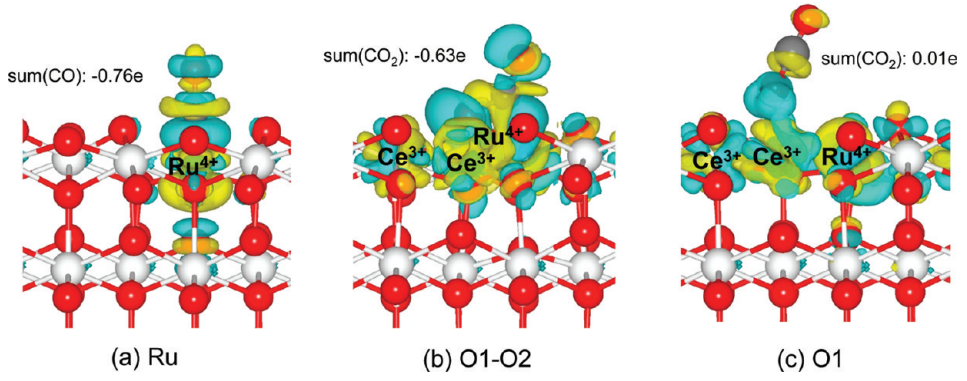

Figure 6. Illustration of charge−density difference for CO oxidation on $Ce_{0.875}Ru_{0.125}O_2(111)$ surface: (a) Ru, (b) O1−O2 (carbonite-like species), (c) O1 (CO_2 formation). $\Delta\rho_{diff}$ isosurfaces were calculated at 0.05 bohr^{-3}. The values are effective charges, which are calculated by the Bader analysis program.

O1−O2, O1−O3, and O2−O3 bridge sites. The adsorbed CO binds to one surface oxygen ion forming a carbonite-like species with the CO tilting from the surface. The adsorption energies for the three carbonite-like species are −2.31, −2.22, and −2.27 eV. The C−O and C−O_{surf} bond distances are 1.20−1.22 and 1.29−1. 32 Å, which are elongated compared to that of a free CO molecule (1.18 Å). A Bader charge analysis gives net charges of −0.63 e (see Figure 6b) for the carbonite-like species and seems to be a reasonable value for a bound CO_2^- ion. The other CO chemisorption is bound to the surface Ru ions with an adsorption energy of −1.56 eV. The C−O and C−Ru bond distances are 1.17 and 1.88 Å, respectively. A Bader charge analysis gives net charges of −0.76 e (see Figure 6a) for this species indicating that a charge transfer from the Ru ion to the CO adsorption. Interestingly, a CO molecule placed at the top of surface O1, O2, and O3 ions (see Figure 1d) neighboring the substitutional Ru^{4+} ion leads to the formation of CO_2 floating on the surface with an oxygen vacancy left in the surface. The process releases −2.31, −2.67, and −2.74 eV for a CO at the top of surface of O1, O2, and O3, see Table 3. The nature of the adsorbed CO_2 species is similar to a free CO_2 molecule with C−O bond distances close to 1.20 Å and the O−C−O angle of almost 180°. In view of the interactions between the CO_2 molecule and the reduced $Ce_{0.875}Ru_{0.125}O_2(111)$ surface, the CO_2 molecule is weakly bound to the surface with the desorption energies of 0.29−0.47 eV.

The reaction mechanisms for CO oxidation and catalyst regeneration are depicted in Figure 7, consisting of three steps: (a) the oxidation of the first CO molecule on the stoichiometric $Ce_{0.875}Ru_{0.125}O_2(111)$ surface through participation of a lattice oxygen, leading to O vacancy formation and CO_2 desorption (Figure 7a); (b) the adsorption of molecular O_2 at the O vacancy, leading to the formation of surface O adspecies (Figure 7b); and (c) the interaction of a CO molecule with these O adspecies, which drives CO oxidation and regeneration of the stoichiometric $Ce_{0.875}Ru_{0.125}O_2$ surface (Figure 7c). Two reaction pathways of the first CO oxidation are considered: the Langmuir−Hinshelwood (LH) and Eley−Rideal (ER) mecha-

dx.doi.org/10.1021/jp210864m | J. Phys. Chem. C 2012, 116, 6239−6246

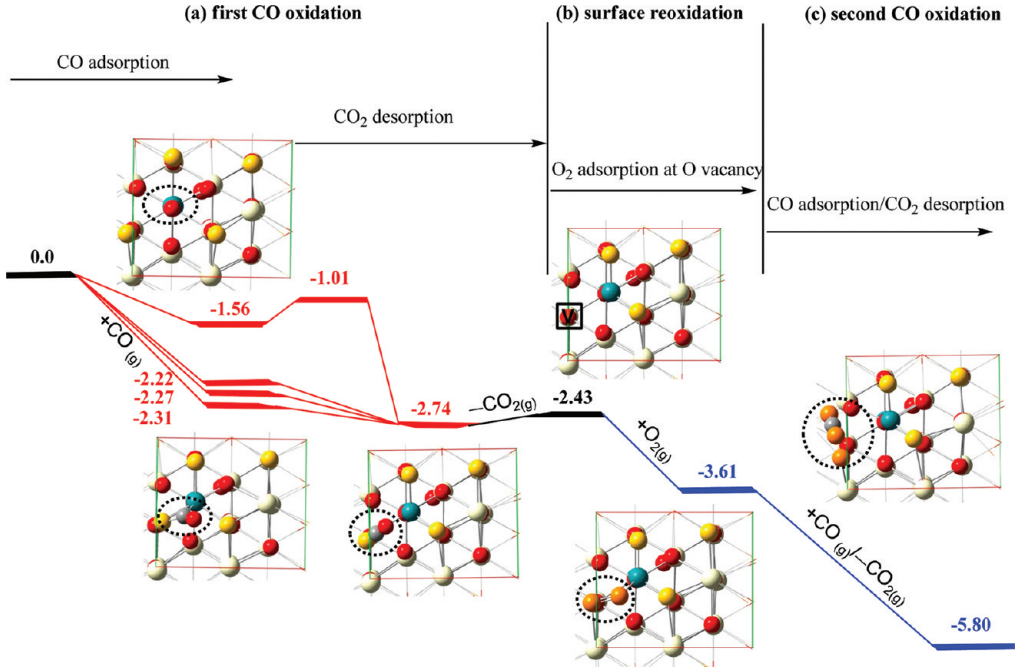

Figure 7. Calculated potential energy diagram for CO oxidation on $Ce_{0.875}Ru_{0.125}O_2$ and catalyst regeneration. The proposed catalytic cycle involves (a) the oxidation of the first CO molecule on the stoichiometric $Ce_{0.875}Ru_{0.125}O_2(111)$ surface through CO adsorption and CO_2 desorption; (b) the adsorption of molecular O_2 at the O vacancy, leading to the formation of surface O adspecies; and (c) the interaction of a CO molecule with these O adspecies, which drives CO oxidation and regeneration of the stoichiometric $Ce_{0.875}Ru_{0.125}O_2$ surface.

nisms as shown in Figure 7. The LH mechanism starts from adsorption of CO with adsorption energies of −2.31, −2.27, and −2.22 eV forming carbonite-like intermediates, which directly produce to the adsorption of CO_2 with exothermicities of 0.43, 0.47, and 0.52 eV. The other possible LH mechanism starts from the CO adsorbed at the Ru-top site with an adsorption energy of −1.56 eV. Then, it overcomes a barrier of 0.55 eV to form the adsorption of CO_2. The ER mechanism can take place directly by abstracting the surface oxygen ions neighboring the substitutional Ru^{4+} ion and leads to the formation of CO_2. The process releases −2.74 eV. The desorption of CO_2 with the formation of a surface O vacancy and reducing the neighboring two Ce^{4+} ions to two Ce^{3+} ions requires only 0.31 eV. On the basis of Bader charge population analysis (see Figure 6), we interpret the Ru ion as Ru^{4+} along the most possible mechanism of CO oxidation via the carbonite-like intermediates, while the two neighbor Ce ions reduce to Ce^{3+} ions. In addition, we also consider second oxidation via the ER mechanism on the reduced substrate after the release of the oxidation of a CO molecule. The second oxidation has no activation barrier, is less exothermic (−2.24 eV) than the first one, and results in the formation of a second O vacancy neighboring to a Ru ion. Our calculation results agree with the experimental observation[20] that $Ce_{1-x}Ru_xO_{2-\delta}$ shows higher OSC and higher percentages of CO oxidation at lower temperature. The reduced catalysts can be sealed by an O_2 molecule from the gas phase. The adsorption energy of the O_2 molecule on the O vacancy is calculated to be −1.18 eV. The O−O bond length has elongated from the O_2 gas phase value of 1.21 Å to 1.38 Å, and the Ce^{3+} ion of the surface reoxidized to Ce^{4+}. The O_2 adsorption is assigned to be peroxide according to the predicted vibrational frequency of 796 cm^{-1}.[50] The resulting O adspecies are active and can promote the direct oxidation of a CO molecule leading to the formation of CO_2, which desorbs without any activation barrier and is exothermic by 2.19 eV (see Figure 7c). The Bader charge analysis for the CO oxidation and catalyst regeneration via healing the vacancy by molecular O_2 on the $Ce_{0.875}Ru_{0.125}O_2(111)$ surface shows a catalytic cycle in which the positive oxidation state of the substitutional Ru ion is preserved throughout the reaction.

3.2.2. Vibrational Spectra Calculations. The vibrational frequencies for the adsorbed species on the $Ce_{0.875}Ru_{0.125}O_2(111)$ surface were estimated as summarized in Table 3. For CO on the $Ce_{0.875}Ru_{0.125}O_2(111)$ surface, the predicted vibrational frequencies at the region of 2112−2157 cm^{-1} are attributed to the C−O stretching of CO physisorption in which the values are close to that of a gas-phase CO molecule (2136 cm^{-1}). However, the predicted C−O frequencies of carbonite-like species (1683, 1847, and 1861 cm^{-1}) are in close agreement with the experimental value,[51,52] 1728 cm^{-1}. The strong red shift of −270 to −450 cm^{-1} with respect to the gas phase CO molecule are similar to the observation in experiments for ceria powder with carbonate species and in the theoretical calculations for the $CeO_2(110)$ surface by Yang et al.,[48] Herschend et al.,[53] and Nolan et al.[54] The vibration mode of CO chemisorption at 1972 cm^{-1} is assigned to linearly bonded CO on the Ru-top site. The estimated vibrational frequencies for the antisymmetric stretching mode, symmetric stretching mode, and bending mode of the adsorbed CO_2 species are in the region of 2371−2429, 1324−1354, and 607−633 cm^{-1}, see Table 3. Compared to those of a gas phase CO_2 (2377, 1321, and 644 cm^{-1}), the frequency shifts of the adsorbed CO_2 species are seen to be very small, indicating and confirming that, indeed, the new adsorption species is likely a weakly adsorbed CO_2 species. In addition, we also calculated vibrational frequency of CO adsorbed on the $Ru/CeO_2(111)$ surface. The estimated vibrational frequency 1980 cm^{-1} is assigned to linearly bonded

dx.doi.org/10.1021/jp210864m | J. Phys. Chem. C 2012, 116, 6239−6246

CO on Ru of the Ru−ceria interface, which is similar to those on Pt/CeO_2 catalyst (1970−1960 and 2054 cm^{-1}).[4]

4. CONCLUSIONS

In summary, we provide insight into the interactions of CO with a Ru-doped CeO_2(111) surface as well as the catalytic mechanisms for CO oxidation by using periodic DFT + U calculations. The key conclusions are summarized as follows: (i) the Ru dopant facilitates oxygen vacancy formation, while the Ru adatoms may suppress oxygen vacancy formation. (ii) Physisorbed CO, physisorbed CO_2, and chemisorbed CO (carbonite, CO_2^-) species are observed on the Ru-doped CeO_2(111) surface, in contrast, only physisorbed CO is found on the clean CeO_2(111) surface. The vibrational frequency calculations are carried to characterize these species. (iii) Incorporating Ru ions into the ceria lattice as substitutional point defects can instead sustain a full catalytic cycle for CO oxidation and catalyst regeneration. The Ru dopant promotes CO oxidation without any activation energy leading to O vacancy formation and CO_2 desorption. Molecular O_2 adsorbs at the O vacancy forming O adspecies that then drive CO oxidation and recover the stoichiometric Ru-doped CeO_2 surface. The Bader charge analysis is carried out to characterize the oxidation state of Ru as +IV ions along the catalytic cycle. These results rationalize the experimental observation[20] that $Ce_{1-x}Ru_xO_{2-\delta}$ shows higher OSC and higher percentages of CO oxidation at lower temperature.

AUTHOR INFORMATION

Corresponding Author

*E-mail: htchen@cycu.edu.tw.

Notes

The authors declare no competing financial interest.

ACKNOWLEDGMENTS

We are grateful to National Science Council, Republic of China, under Grant Number NSC 99-2113-M-033-009-MY2 and Taiwan National Center for Theoretical Sciences (NCTS) for the financial support, and National Center for High-performance Computing, Taiwan, for the computer time and facilities.

REFERENCES

(1) Bourane, A.; Bianchi, D. *J. Catal.* **2001**, *202*, 34.
(2) Bunluesin, T.; Gorte, R. J.; Graham, G. W. *Appl. Catal., B* **1997**, *14*, 105.
(3) Gamarra, D.; Belver, C.; Fernández-Garcia, M.; Martínez-Arias, A. *J. Am. Chem. Soc.* **2007**, *129*, 12064.
(4) Pozdnyakova, O.; Teschner, D.; Wootsch, A.; Kröhnert, J.; Steinhauer, B.; Sauer, H.; Toth, L.; Jentoft, F. C.; Knop-Gericke, A.; Paal, Z.; Schlogl, R. *J. Catal.* **2006**, *237*, 1.
(5) Trovarelli, A. *Catalysis by Ceria and Related Materials*; Imperial College Press: London, U.K., 2002.
(6) Aneggi, E.; Llorca, J.; Boaro, M.; Trovarelli, A. *J. Catal.* **2005**, *234*, 88.
(7) Huang, M.; Fabris, S. *J. Phys. Chem. C* **2008**, *112*, 8643.
(8) Nolan, M.; Watson, G. W. *J. Phys. Chem. B* **2006**, *110*, 16600.
(9) Yang, Z.; Woo, T. K.; Baudin, M.; Hermansson, K. *J. Chem. Phys.* **2004**, *120*, 7741.
(10) Shapovalov, V.; Metiu, H. *J. Catal.* **2007**, *245*, 205.
(11) Camellone, M. F.; Fabris, S. *J. Am. Chem. Soc.* **2009**, *131*, 10473.
(12) Yang, Z.; He, B.; Lu, Z.; Hermansson, K. *J. Phys. Chem. C* **2010**, *114*, 4486.
(13) Nolan, M. *J. Phys. Chem. C* **2009**, *113*, 2425.
(14) Yeriskin, I.; Nolan, M. *J. Chem. Phys.* **2009**, *131*, 244702.
(15) Bueno-Lopez, A.; Krishna, K.; Makkee, M.; Moulijn, J. A. *Catal. Today* **2007**, *121*, 237.
(16) Fierro-Gonzales, J. C.; Gates, B. C. *Catal. Today* **2007**, *122*, 201.
(17) Hernández, W. Y.; Centeno, M. A.; Romero-Sarria, F.; Odriozola, J. A. *J. Phys. Chem. C* **2009**, *113*, 5629.
(18) Patil, S.; Seal, S.; Guo, Y.; Schulte, A.; Norwood, J. *Appl. Phys. Lett.* **2006**, *88*, 243110.
(19) Wang, X.; Rodriguez, J. A.; Hanson, J. C.; Gamarra, D.; Martinez-Arias, A.; Fernandez-Garcia, M. *J. Phys. Chem. B* **2005**, *109*, 19595.
(20) Singh, P.; Hegde, M. S. *Chem. Mater.* **2009**, *21*, 3337.
(21) Kresse, G.; Hafner, J. *Phys. Rev. B* **1993**, *47*, 558.
(22) Kresse, G.; Furthmüller, J. *Phys. Rev. B* **1996**, *54*, 11169.
(23) Blöchl, P. E. *Phys. Rev. B* **1994**, *50*, 17953.
(24) Perdew, J. P.; Burke, K.; Ernzerhof, M. *Phys. Rev. Lett.* **1996**, *77*, 3865.
(25) Perdew, J. P.; Chevary, J. A.; Vosko, S. H.; Jackson, K. A.; Pederson, M. R.; Singh, D. J.; Fiolhais, C. *Phys. Rev. B* **1992**, *46*, 6671.
(26) Perdew, J. P.; Wang, Y. *Phys. Rev. B* **1992**, *45*, 13244.
(27) Monkhorst, H. J.; Pack, J. D. *Phys. Rev. B* **1976**, *13*, 5188.
(28) Nolan, M.; Grigoleit, S.; Sayle, D. C.; Parker, S. C.; Watson, G. W. *Surf. Sci.* **2005**, *576*, 217.
(29) Nolan, M.; Parker, S. C.; Watson, G. W. *Surf. Sci.* **2005**, *595*, 223.
(30) Fabris, S.; de Gironcoli, S.; Baroni, S.; Vicario, G.; Balducci, G. *Phys. Rev. B* **2005**, *71*, 041102.
(31) Fabris, S.; Vicario, G.; Balducci, G.; de Gironcoli, S.; Baroni, S. *J. Phys. Chem. B* **2005**, *109*, 22860.
(32) Dudarev, S. L.; Botton, G. A.; Savrasov, S. Y.; Humphreys, C. J.; Sutton, A. P. *Phys. Rev. B* **1998**, *57*, 1505.
(33) Chen, H.-T.; Choi, Y. M.; Liu, M.; Lin, M. C. *ChemPhysChem* **2007**, *8*, 849.
(34) Loschen, C.; Carrasco, J.; Neyman, K. M.; Illas, F. *Phys. Rev. B* **2007**, *75*, 035115.
(35) Andersson, D. A.; Simak, S. I.; Johansson, B.; Abrikosov, I. A.; Skorodumova, N. V. *Phys. Rev. B* **2007**, *75*, 035109.
(36) Chen, H.-L.; Chang, J.-C.; Chen, H.-T. *Chem. Phys. Lett.* **2011**, *502*, 169.
(37) Chen, H.-T.; Chang, J.-C. *J. Chem. Phys.* **2010**, *132*, 214702.
(38) Jiang, Y.; Adams, J. B.; Schilfgaarde, M. V. *J. Chem. Phys.* **2005**, *123*, 064701.
(39) Chen, H.-T.; Chang, J.-C. *J. Phys. Chem. C* **2011**, *115*, 14745.
(40) Hill, S. E.; Catlow, C. R. A. *J. Phys. Chem. Solids* **1993**, *54*, 411.
(41) Kummerle, E. A.; Heger, G. *J. Solid State Chem.* **1999**, *147*, 485.
(42) Skorodumova, N. V.; Ahuja, R.; Simak, S. I.; Abrikosov, I. A.; Johansson, B.; Lundqvist, B. I. *Phys. Rev. B.* **2001**, *64*, 115108.
(43) Yang, Z. X.; Woo, T. K.; Baudin, M.; Hermansson, K. *J. Chem. Phys.* **2004**, *120*, 7741.
(44) Lyons, D. M.; Ryan, K. M.; Morris, M. A. *J. Mater. Chem.* **2002**, *12*, 1207.
(45) Lyons, D. M.; McGrath, J. P.; Morris, M. A. *J. Phys. Chem. B* **2003**, *107*, 4607.
(46) Mills, G.; Jönsson, H.; Schenter, G. *Surf. Sci.* **1995**, *324*, 305.
(47) Henkelman, G.; Uberuaga, B. P.; Jönsson, H. *J. Chem. Phys.* **2000**, *113*, 9901.
(48) Yang, Z.; Woo, T. K.; Hermansson, K. *Chem. Phys. Lett.* **2004**, *396*, 384.
(49) Lin, W. F.; Zei, M. S.; Kim, Y. D.; Over, H.; Ertl, G. *J. Phys. Chem. B* **2000**, *104*, 6040.
(50) Chen, H.-T.; Chang, J.-C.; Chen, H.-L.; Ju, S.-P. *J. Comput. Chem.* **2009**, *30*, 2433.
(51) Li, C.; Sakata, Y.; Arai, T.; Domen, K.; Maruya, K.; Onishi, T. *J. Chem. Soc., Faraday Trans. 1* **1989**, *85*, 929.
(52) Li, C.; Sakata, Y.; Arai, T.; Domen, K.; Maruya, K.; Onishi, T. *J. Chem. Soc., Faraday Trans. 1* **1989**, *85*, 1451.
(53) Herschend, B.; Baudin, M.; Hermansson, K. *Chem. Phys.* **2005**, *328*, 345.
(54) Nolan, M.; Parker, S. C.; Watson, G. W. *Surf. Sci.* **2006**, *600*, 175.